IEEE Access
Multidisciplinary | Rapid Review | Open Access Journal

Received January 20, 2020, accepted February 13, 2020, date of publication February 20, 2020, date of current version March 2, 2020.

Digital Object Identifier 10.1109/ACCESS.2020.2975430

Performance of GFDM Systems Using Quadratic Programming Pulse Shaping Filter Design

ZEE ANG SIM, (Member, IEEE), FILBERT H. JUWONO, (Senior Member, IEEE), REGINA REINE, (Member, IEEE), ZHUQUAN ZANG, (Member, IEEE), AND LENIN GOPAL, (Member, IEEE)

Department of Electrical and Computer Engineering, Curtin University Malaysia, Miri 98009, Malaysia

Corresponding author: Zee Ang Sim (zee.ang@postgrad.curtin.edu.my)

This work was supported by the Fundamental Research Grant Scheme (FRGS) from the Ministry of Higher Education, Malaysia, under Grant FRGS/1/2017/TK04/CURTIN/03/1.

ABSTRACT Generalized Frequency Division Multiplexing (GFDM) has been considered as an attractive candidate to replace Orthogonal Frequency Division Multiplexing (OFDM) for the fifth generation (5G) mobile networks. GFDM system has better spectral characteristics compared to the OFDM system due to the use of properly selected pulse shaping filters. Non-causal ideal filters, such as the raised cosine (RC), are commonly used in the GFDM systems. In practical implementation, non-causal filters need to be truncated and shifted, which will increase the out-of-band (OOB) radiation of the signal and will introduce delay to the system. High OOB radiation will cause interferences between the adjacent channels, thus it should be minimized. This paper proposes to minimize the OOB radiation of the GFDM system using the designed pulse shaping filters. The pulse shaping filters are designed using the computationally efficient quadratic programming (QP) approach. Numerical results illustrate that OOB radiation level of the GFDM system is lower when the QP filters are used compared to the conventional RC filter. Further investigation shows that the use of the QP filters are efficient in increasing the high power amplifier (HPA) efficiency, improving the spectral efficiency, and reducing the BER at the receiver.

INDEX TERMS 5G, filter design, GFDM, HPA, nonlinearity, OOB radiation, PAPR, quadratic programming.

I. INTRODUCTION

Due to the high spectral efficiency and the robustness to multipath fading channels, Orthogonal Frequency Division Multiplexing (OFDM) system has been widely applied in the current fourth generation (4G) wireless communication standards, such as the Long Term Evolution - Advanced (LTE-A), Worldwide Interoperability for Microwave Access (WiMAX), asymmetric digital subscriber line (ADSL), digital audio broadcasting (DAB), and digital video broadcasting (DVB) [1]–[3]. Recently, it is envisaged that fifth generation (5G) will be the next communication standards that supports emerging applications with more diverse requirements and specifications [4]. The Internet of Things (IoT) is expected to be one of the key applications in the 5G, where up to 100,000 devices and sensor modules may connect to a single base station [5]. The high out-of-band (OOB) radiation of the OFDM system becomes one of the major drawbacks for its implementation as the suitable modulation technique for 5G communication systems because the high OOB will cause interferences between the adjacent channels. To satisfy the spectral regulatory masks, the OOB radiation of the transmitted signal for the 5G base stations must be below the required limits, i.e., −45 dB [6].

Rectangular filter is used in the OFDM system and its amplitude has abrupt discontinuity which induces spectral growth and lead to the high OOB radiation. One of the simple techniques to minimize the OOB radiation of the OFDM signal is time windowing [7]–[9]. Time windowing allows a smooth transition between OFDM symbols by varying the amplitudes at the edges gradually towards zero. However, windowing requires extra bandwidth and hence, reduces the spectral efficiency. Another well-researched technique is the use of cancellation carriers (CC), where a subset

The associate editor coordinating the review of this manuscript and approving it for publication was Mingjun Dai.

of subcarriers are weighted to suppress the OOB [10], [11]. However, this technique reduces the spectral efficiency as the subcarriers do not contain any useful information and waste the bandwidth.

Due to the above-mentioned OFDM issues, several multicarrier modulation techniques have been proposed as potential candidates for the 5G mobile networks, such as Filter Bank Multicarrier (FBMC), Universal Filtered Multicarrier (UFMC), and Generalized Frequency Division Multiplexing (GFDM) [5], [12]–[14]. The FBMC system shapes each subcarrier with a narrowband filter. However, it has a long impulse response which is not suitable for sporadic traffic from the IoT devices. UFMC does not require cyclic prefix (CP) and it uses filtering over a group of subcarriers which are good for spectral efficiency. However, UFMC requires strict time-synchronization to reduce inter-symbol interference (ISI).

Recently, the GFDM has been considered as one of the promising candidates in replacing the OFDM system for the 5G communication system. In GFDM, the data symbols are shaped by a prototype filter that is shifted circularly in time and frequency domains. On top of the advantageous properties of OFDM systems, GFDM systems are well-suited for different 5G scenarios by flexibly manipulating the system parameters, which consists of subcarriers, subsymbols, and the pulse shaping filters. Existing ideal pulse shaping filters such as the raised cosine (RC) and root raised cosine (RRC) are usually used in the GFDM system [14]–[17]. Ideal filters are non-causal and practically unrealizable . Truncation and shifting can be performed but this will cause spectral regrowth in the OOB region and will introduce delay in the system.

There is still lack of thorough investigation in designing filter for the GFDM system, particularly when the signal is passed through the high power amplifier (HPA). In [18], a prototype filter with spectral emission mask (SEM) constraint is designed. However, it uses an iterative algorithm which causes high complexity, and the performance improvement is relatively small. In [19], an optimization problem which minimizes the power spectral density (PSD) of the GFDM filtering matrix in the OOB region is formulated, but numerical results presented only covers low numbers of subcarriers and subsymbols which are not applicable in practical systems. Using the quadratic programming (QP) optimization approach to design the filter for the OFDM system is proposed in [20]. Based on [20], a similar approach of the filter design for the GFDM system is investigated in [21] and [22]. However, there is lack of investigation in minimizing the OOB radiation when the transmitted GFDM signal is passed through the HPA.

This paper proposes to minimize the OOB radiation of the GFDM system using the pulse shaping filters designed via the computationally efficient QP optimization approach. The QP designed filter has been discussed in [21] and [22]. However, practical GFDM systems use the HPA which is not considered in [21] and [22]. In particular, this paper focuses on presenting a holistic investigation of the performance of the designed pulse shaping filters in GFDM systems from an amplifier efficiency and nonlinearity perspective. In practice, a HPA is commonly employed at the transmitter. The transmit signal is passed to the HPA before being transmitted to the communication channel. As an HPA is a nonlinear device, it may change the characteristics of the system performance, especially when the HPA operates in the nonlinear region. In particular, nonlinear characteristic may lead to spectral regrowth and bit error rate (BER) degradation due to high peak-to-average power ratio (PAPR) [23], [24]. It is worth mentioning that GFDM signal has a relatively high PAPR as shown in [21], [25]. This work thus provides an in-depth investigation on the impact of HPA nonlinearity in a GFDM system, and the performance of the designed practical filter against an ideal filter in such a scenario. To the best of the authors' knowledge, a thorough analysis of GFDM system performance in presence of a nonlinear HPA has not been available in the literature.

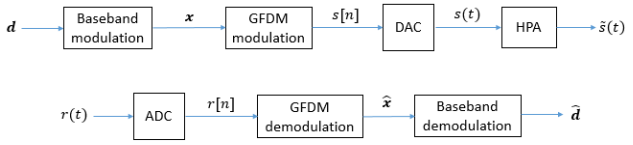

FIGURE 1. GFDM transmitter and receiver system model.

To summarize, the main objective of this paper is to use the QP approach to design a practically realizable pulse shaping filter which reduces the OOB emission in GFDM systems in order to meet the 5G specification. The performance of the QP-GFDM system under the nonlinearity effect of the HPA in terms of OOB radiation, BER, and PAPR is investigated. The performance is analyzed and compared with the one of RC-GFDM and OFDM. The energy efficiency of the HPA and overall system performance with HPA is also presented.

The remaining sections of this paper are structured as follows. Section II presents a low complexity GFDM transmitter and receiver structure, as well as the HPA model considered. In Section III, the mathematical description of the OOB radiation in GFDM signals is given. This is followed by the problem formulation of designing a pulse shaping filter which minimizes stopband leakage in Section IV. The metrics to analyze the performance of the designed pulse shaping filter in a GFDM system considering HPA nonlinearity is presented in Section V, and numerical results comparing the designed pulse shaping filter with the ideal RC filter is illustrated and discussed in Section VI. Finally, concluding remarks are given in Section VII.

II. SYSTEM MODEL

A. GFDM TRANSMITTER

Consider a GFDM system as shown in Fig. 1, a total of N input data symbols, denoted as $\mathbf{d} = \{d_0, d_1, \ldots, d_{N-1}\}$, are

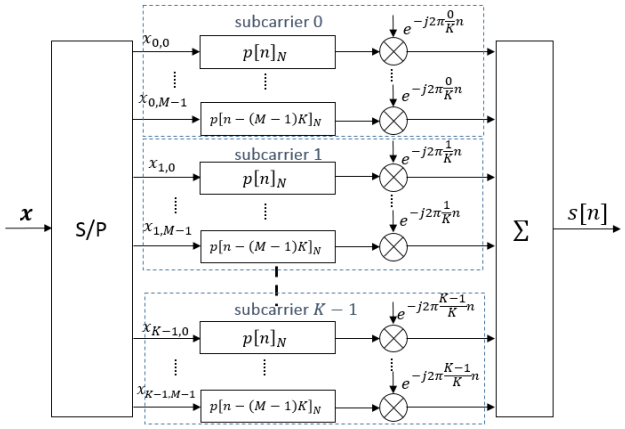

FIGURE 2. GFDM modulator.

baseband modulated using Quadrature Amplitude Modulation (QAM) yielding $\mathbf{x}$. As illustrated in Fig. 2, the GFDM modulator distributes $\mathbf{x}$ into K subcarriers, with each subcarrier carrying M subsymbols, where $N = KM$, and $x_{k,m}$ denotes the data symbol for the kth subcarrier and mth subsymbol. Each data symbol is pulse shaped by a prototype filter, $p_{k,m}[n]$, which also shifts the data symbol to its respective carrier frequency and time slot. The illustrated GFDM transmission operation before being passed through the HPA can be expressed as the weighted superposition of K subcarrier signals given by [26]

$$s[n] = \sum_{k=0}^{K-1} \sum_{m=0}^{M-1} x_{k,m} p_{k,m}[n], \tag{1}$$

where

$$p_{k,m}[n] = p[(n - mK) \text{mod} N] e^{-j2\pi \frac{k}{K} n}, \tag{2}$$

is a time and frequency shifted version of a prototype pulse shaping filter $p[n]$.

The GFDM equation in (1) can be expressed in the frequency domain based on sparse frequency domain processing which has a significantly lower complexity, and is given by [26]

$$\mathbf{s} = \mathbf{W}_N^H \sum_{k=0}^{K-1} \mathbf{\Psi}_k \mathbf{P} \mathbf{\Lambda} \mathbf{W}_M \mathbf{x}_k, \tag{3}$$

where $\mathbf{W}_M$ is an M-point discrete Fourier transform (DFT) matrix and $\mathbf{\Lambda} = \{\mathbf{I}_M \mathbf{I}_M \ldots\}$ is a concatenation of V identity matrices. The parameter V is the upsampling factor of the pulse shaping filter and $V = 2$ is sufficient for most pulse shaping filters [26]. The filter matrix $\mathbf{P} = \text{diag}\{P_0, P_1, \ldots, P_{N-1}\}$ is a diagonal matrix with entries from the frequency response coefficients of the prototype filter. A permutation matrix $\mathbf{\Psi}_k$ is used to up-convert each subcarrier to their respective frequencies according to the following:

$$\mathbf{\Psi}_0 = \begin{pmatrix} \mathbf{I}_{QM/2} & \mathbf{0}_{QM/2} & \ldots & \mathbf{0}_{QM/2} & \mathbf{0}_{QM/2} \\ \mathbf{0}_{QM/2} & \mathbf{0}_{QM/2} & \ldots & \mathbf{0}_{QM/2} & \mathbf{I}_{QM/2} \end{pmatrix}^{\mathrm{T}}$$
$$\mathbf{\Psi}_1 = \begin{pmatrix} \mathbf{0}_{QM/2} & \mathbf{I}_{QM/2} & \ldots & \mathbf{0}_{QM/2} & \mathbf{0}_{QM/2} \\ \mathbf{I}_{QM/2} & \mathbf{0}_{QM/2} & \ldots & \mathbf{0}_{QM/2} & \mathbf{0}_{QM/2} \end{pmatrix}^{\mathrm{T}}$$
$$\vdots$$
$$\mathbf{\Psi}_{K-1} = \begin{pmatrix} \mathbf{0}_{QM/2} & \mathbf{0}_{QM/2} & \ldots & \mathbf{0}_{QM/2} & \mathbf{I}_{QM/2} \\ \mathbf{0}_{QM/2} & \mathbf{0}_{QM/2} & \ldots & \mathbf{I}_{QM/2} & \mathbf{0}_{QM/2} \end{pmatrix}^{\mathrm{T}}. \tag{4}$$

Finally, all subcarrier signals are superpositioned and converted into the time domain using the inverse discrete Fourier transform (IDFT) matrix $\mathbf{W}_N^H$, where $(\cdot)^H$ denotes Hermitian.

After converting the discrete-time GFDM signal, $s[n]$, into a continuous time signal, $s(t)$, via a digital-to-analog converter (DAC), the signal is passed to a HPA before the actual transmission. Let $s(t) = r(t)e^{j\phi(t)}$ denote the baseband representation of the input signal to the HPA, where $r(t) = |s(t)|$ is a positive continuous random variable denoting the envelope of $s(t)$ and $\phi(t)$ denotes the phase at a given time instant, t. The output of the HPA is given by [27]

$$\tilde{s}(t) = g(r(t))e^{j\Phi(r(t))}e^{j\phi(t)}, \tag{5}$$

where $g(r)$ and $\Phi(r)$ are the time-domain envelope and phase responses commonly referred to as AM-AM and AM-PM characteristics, respectively, for a given instantaneous envelope, r.

In this paper, the Rapp's model [28] is used to represent a practical memoryless solid-state power amplifier (SSPA) model. The Rapp's model is commonly used for simulating nonlinearity models [29]–[32] and is also used in evaluating the 5G-NR [33]. The AM-AM characteristic of the Rapp's model can be expressed as

$$g(r) = r_{out} = r_{out,max} \frac{\frac{r_{in}}{r_{in,max}}}{\left(1 + \left(\frac{r_{in}}{r_{in,max}}\right)^{2p}\right)^{\frac{1}{2p}}}, \tag{6}$$

and the AM-PM characteristic is assumed to be insignificant, which can be expressed as

$$\Phi(r) = 0. \tag{7}$$

Parameter p is a positive value that controls the smoothness of the curve, with $p \to \infty$ corresponding to an ideally linearized model. The normalized output of a Rapp's model with respect to different p is as shown in Fig. 3. Parameter r_{in} denotes the input envelope to the HPA, $r_{\text{in,max}}$ is the maximum saturation point of the HPA input, r_{out} is the output envelope from the HPA, and $r_{\text{out,max}}$ is the maximum saturation point of the HPA output.

B. GFDM RECEIVER STRUCTURE

At the receiver, the discrete received signal can be expressed as

$$y[n] = h[n] * \tilde{s}[n] + z[n], \tag{8}$$

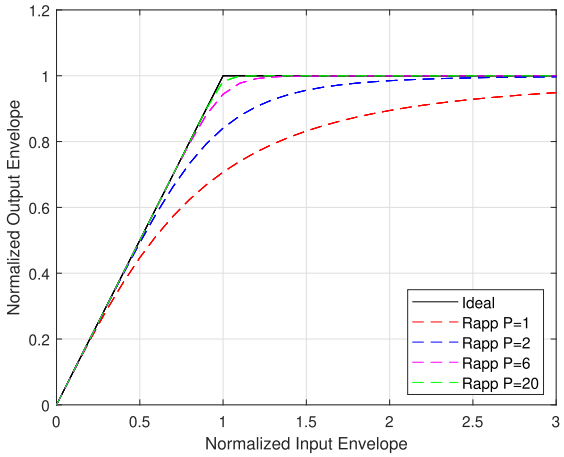

FIGURE 3. AM-AM characteristics of the Rapp's Model with several smoothness factors *p*.

where $h[n]$ is the channel impulse response, $\tilde{s}[n]$ is the discrete output signal from the HPA, $z[n]$ is the additive white Gaussian noise (AWGN), and $*$ denotes convolution.

The received signal, $y[n]$, is represented in a vector as $\mathbf{y} = \{y_0, y_1, \ldots, y_{N-1}\}$, followed by conversion to the frequency domain with $\mathbf{Y} = \mathbf{W}_N\mathbf{y}$. To compensate for distortions from the channel and AWGN, the minimum mean-squared error (MMSE) equalizer can be applied, and can be expressed as

$$\hat{\mathbf{Y}} = \mathbf{\Gamma}\mathbf{Y}, \tag{9}$$

where $\mathbf{\Gamma} = \text{diag}\{\gamma, \gamma_1, \ldots, \gamma_{N-1}\}$ is an $N \times N$ diagonal matrix with entries from the weighting parameters of MMSE. The data symbols of each subcarrier can then be recovered from the equalized signal via

$$\hat{\mathbf{x}}_k = \mathbf{W}_M^{\mathrm{H}}\mathbf{\Lambda}^{\mathrm{T}}\mathbf{P}^{\mathrm{H}}\mathbf{\Psi}^{\mathrm{T}}\hat{\mathbf{Y}}. \tag{10}$$

III. POWER SPECTRAL DENSITY

The PSD of a baseband signal is derived according to [34] as follows

$$PSD(f) = \lim_{T\to\infty}\frac{1}{T}E\{|s(t)e^{-j2\pi ft}dt|\}, \tag{11}$$

where $s(t)$ is obtained from the GFDM transmit signal, $s[n]$, that is fed to a DAC and truncated to the interval $(-T/2, T/2)$.

In the GFDM case, the PSD of $s(t)$ is measured across v number of GFDM blocks, each ranges from $-\frac{T}{2MT_s}$ to $+\frac{T}{2MT_s}$, where T_s is the time duration of one subsymbol. The analog baseband signal is obtained as

$$s(t) = \sum_{v,m,k} X_{v,m,k}p_{0,m}(t - vMT_s)e^{-j2\pi\frac{k}{T_s}t}, \tag{12}$$

with the frequency domain representation written as

$$S(f) = \sum_{v,m,k} X_{v,m,k}P_m\Big(f - \frac{k}{T_s}\Big)e^{-j2\pi vMT_sf}, \tag{13}$$

where $P_m(f)$ is the Fourier transform of $p_{0,m}$. Assuming that the data symbols are zero-mean and independent and identically-distributed (i.i.d.), the PSD of a GFDM system can be obtained by substituting (13) into (11), which can be expressed as [15]

$$PSD_{GFDM}(f) = \frac{1}{MT_s}\sum_{k,m}\Big|P_m\Big(f - \frac{k}{T_s}\Big)\Big|^2. \tag{14}$$

The OOB leakage can be analyzed by using the ratio of the average energy that is emitted into neighbouring frequency bands and the average energy within the allocated bandwidth. It is defined as [15]

$$\mathcal{O} = \frac{|\mathcal{B}|}{|\mathcal{OOB}|}\cdot\frac{\int_{f\in\mathcal{OOB}}PSD(f)df}{\int_{f\in\mathcal{B}}PSD(f)df}, \tag{15}$$

where $|\mathcal{B}|$ and $|\mathcal{OOB}|$ are the cardinality of the in-band frequencies and the out-of-band frequencies, respectively.

To prevent interferences to the neighbouring channels, the OOB radiation should be suppressed to a desirable level [6]. Based on (15), it can be seen that the OOB radiation can be reduced by minimizing the stopband energy of the pulse shaping filter.

IV. PULSE SHAPING FILTER DESIGN

The frequency response of an R-tap FIR pulse shaping filter can be written as

$$P(e^{j\omega}) = \sum_{r=0}^{R-1}h_re^{-j\omega r} = \mathbf{h}^{\mathrm{T}}\mathbf{e}(\omega), \tag{16}$$

given that $\mathbf{h} = [h_0, h_1, \ldots, h_{(R-1)}]^{\mathrm{T}}$ are the impulse response coefficients of the designed filter, $\mathbf{e}(\omega) = [1, e^{-j\omega}, \ldots, e^{-j\omega(R-1)}]^{\mathrm{T}}$, and $\omega = 2\pi f$ where f is the linear frequency in Hz.

A. PROBLEM FORMULATION

To minimize the stopband energy of the pulse shaping filter, the optimization problem can be formulated as

$$\min_{\mathbf{h}}\frac{1}{\pi}\int_{\Omega_s}\lambda(\omega)|P(e^{j\omega}) - P_d(\omega)|^2d\omega,$$
subject to (17)

$$|P(e^{j\omega}) - P_d(\omega)| \le \sigma_p, \quad \omega\in\Omega_p, \tag{18}$$

where $\lambda(\omega)$ is a positive weighting function, $P_d(\omega)$ is the frequency response of the desired filter, Ω_s and Ω_p are the set of stopband and passband frequencies, respectively, and σ_p is the error tolerance in the passband. Note that $\lambda(\omega)$ is defined by the designer. In view of (17) and (18), the optimization problem can be reformulated and solved using the QP approach.

B. PROBLEM SIMPLIFICATION

The objective function (17) can be simplified as

$$\min_{\mathbf{h}}\Big\{\frac{1}{2}\mathbf{h}^{\mathrm{T}}\xi\mathbf{h} - v^{\mathrm{T}}\mathbf{h}\Big\}, \tag{19}$$

where

$$\xi = \frac{2}{\pi}\int_{\Omega_s} \lambda(\omega)\mathbf{e}(\omega)\mathbf{e}^{\mathrm{H}}(\omega)d\omega,$$
$$\nu = \frac{2}{\pi}\int_{\Omega_s} \lambda(\omega)\Re\{\mathbf{e}(\omega)P_d(\omega)\}d\omega,$$

and $\Re\{\cdot\}$ denotes the real part of the function within.

As the function $P(e^{j\omega})$ is complex, the constraint (18) is nonlinear. It is desirable to linearize the constraint as a nonlinear problem with nonlinear constraint is complex and difficult to solve using existing optimization tools.

To linearize the inequality constraint (18), an additional parameter, θ, is introduced via the real rotation theorem. Eq.(18) can be rewritten as

$$\max_{0\le\theta\le 2\pi} \Re\{(P(e^{j\omega}) - P_d(\omega))e^{j\theta}\} \le \sigma_p, \omega \in \Omega_p, \quad (20)$$

which is equivalent to

$$\Re\{(\mathbf{h}^{\mathrm{T}}\mathbf{e}(\omega) - P_d(\omega))e^{j\theta}\} \le \sigma_p, \quad (21)$$

for $\omega \in \Omega_p$, $\theta \in [0, 2\pi]$. Rearranging (21), the following is obtained

$$\mathbf{h}^{\mathrm{T}}\Re\{\mathbf{e}(\omega)e^{j\theta}\} \le \sigma_p + \Re\{P_d(\omega)e^{j\theta}\}, \quad (22)$$

and can be rewritten as

$$b^{\mathrm{T}}(\omega,\theta)\mathbf{h} \le c(\omega,\theta), \quad (23)$$

where $b(\omega,\theta) = \Re\{\mathbf{e}(\omega)e^{j\theta}\}$, $c(\omega,\theta) = \sigma_p + \Re\{P_d(\omega)e^{j\theta}\}$.

From (23), it can be seen that the new parameter θ is continuous and has increased the number of constraints. In view of (19) and (23), the optimization problem is now a semi-infinite QP problem. The number of variables $\mathbf{h}$ to be optimized is finite, but the number of constraints, which are dependent on ω and θ, are infinite. This can be solved via discretization of the parameters ω and θ using the method in [35]. For simplicity, parameter θ is discretized as a discrete set $\{\theta_i\}_{i=1}^{2q}$ with

$$\theta_i = \frac{\pi(i-1)}{q}, q \ge 2.$$

Furthermore, let us define

$$Y_n^q(\omega) = \max_{1\le i\le 2q} \Re\{(\mathbf{h}^{\mathrm{T}}\mathbf{e}(\omega) - P_d(\omega))e^{j\theta_i}\}. \quad (24)$$

It was shown in [36] that

$$Y_n^q(\omega) \le \max_{0\le\theta\le 2\pi} \Re\{(\mathbf{h}^{\mathrm{T}}\mathbf{e}(\omega) - P_d(\omega))e^{j\theta}\} \le Y_n^q(\omega)\sec\left(\frac{\pi}{2q}\right). \quad (25)$$

When $q \to \infty$, the value of $\sec(\frac{\pi}{2q}) \to 1$, which indicates that $Y_n^q(\omega)$ gives a decent estimate of $P(e^{j\omega})$. In fact, for $q = 8$, $\sec(\frac{\pi}{2q}) = 1.020$. Hence, instead of using (22), the following strengthened inequality constraints over the discrete sets $\{\omega_l\}_{l=1}^{L}$ and $\{\theta_i\}_{i=1}^{2q}$ should be considered

$$\max_{1\le i\le 2q} \Re\{\mathbf{h}^{\mathrm{T}}\mathbf{e}(\omega_l)e^{j\theta}\} \le \frac{\sigma_p}{\sec(\frac{\pi}{2q})} + \Re\{P_d(\omega_l)e^{j\theta}\}. \quad (26)$$

Replacing $\mathbf{e}(\omega_l)$ with $e^{-j\omega_l k}$, (26) becomes

$$\max_{1\le i\le 2q} \mathbf{h}^{\mathrm{T}}\cos(\omega_l k - \theta_i) \le \frac{\sigma_p}{\sec\frac{\pi}{2q}} + P_d(\omega_l)\cos(\theta_i), \quad (27)$$

which can be simplified to the following set of inequality constraints

$$B_l\mathbf{h} \le c_l, \quad (28)$$

where, for each l, B_l is a $2q$ by M matrix with $b^{\mathrm{T}}(\omega_l,\theta_i) = \cos(\omega_l k - \theta_i)$ as its ith row and c_l is a $2q$-dimensional vector with entries acquired with $c_l = \frac{\sigma_p}{\sec\frac{\pi}{2q}} + P_d(\omega_l)\cos(\theta_i)$.

To summarize, the pulse shaping filter design problem (17) and (18) can be simplified to the following QP problem:

Given discrete sets of $\{\theta_i\}_{i=1}^{2p}$ *and* $\{\omega_l\}_{l=1}^{L}$, *find* $\mathbf{h}$ *which solves the following constrained optimization problem*

$$\min_{\mathbf{h}} \left\{\frac{1}{2}\mathbf{h}^{\mathrm{T}}\xi\mathbf{h} - \nu^{\mathrm{T}}\mathbf{h}\right\},$$
subject to
$$B_l\mathbf{h} \le c_l,$$

The now simplified optimization problem can be solved efficiently using existing software such as MATLAB and its Communication and Optimization Toolboxes.

V. SYSTEM PERFORMANCE METRICS

A. PAPR

The PAPR of the baseband transmitted signal, $s[n]$, is defined as the maximum power, $\max\{|s[n]|^2\}$, over the expectation of the signal power, $\mathrm{E}\{|s[n]|^2\}$. It can be expressed as [37]

$$PAPR = \frac{\max_{0\le n<N-1}\{|s[n]|^2\}}{\mathrm{E}\{|s[n]|^2\}}, \quad (29)$$

where $E\{\cdot\}$ denotes expectation.

For large number of subcarriers, the probability of a maximum peak power to occur in multicarrier signals is extremely low. Thus, the PAPR measure in (29) may not give the whole picture about the dynamic variations of multicarrier signals. A more meaningful approach in analyzing the PAPR is by using the complementary cumulative distribution function (CCDF), which computes the probability that the signal exceeds a certain PAPR level, $PAPR_0$. The CCDF of the PAPR can be written as [38]

$$C_{PAPR}(PAPR_0) = Pr(PAPR \ge PAPR_0) = 1 - (1 - \exp^{-PAPR_0})^N. \quad (30)$$

B. HPA EFFICIENCY

The efficiency of the HPA, η, can be expressed as the ratio of the average output power from the HPA, $\mathcal{P}_{out} = E\{r_{out}^2\}$, to the DC power supplied to the HPA, $\mathcal{P}_{DC}$, and can be written as [27]

$$\eta = \frac{\mathcal{P}_{out}}{\mathcal{P}_{DC}}. \quad (31)$$

In general, the value of η depends on the class of the HPA. In this paper, the Class-A and Class-B HPAs are considered as

they are commonly used for mobile terminals. The efficiency of the Class-A, η_A, and Class-B HPA, η_B, are respectively given by [39]

$$\eta_A = \frac{1}{2}\frac{E\{r_{out}^2\}}{r_{out,max}^2}, \tag{32}$$

and

$$\eta_B = \frac{\pi}{4}\frac{E\{r_{out}^2\}}{r_{out,max}E\{r_{out}\}}. \tag{33}$$

The efficiency of the HPA can be improved by scaling the signal input power such that the signal is within the linear region and not exceeding the saturation point. This can be done by applying an input backoff (IBO) to the input signal, which is given by [39]

$$\text{IBO} \triangleq \frac{r_{in,max}^2}{\mathcal{P}_{in}}, \tag{34}$$

where $\mathcal{P}_{in} = E\{r_{in}^2\}$ denotes the average input power. Similarly, the output backoff (OBO) can be defined as

$$\text{OBO} \triangleq \frac{r_{out,max}^2}{\mathcal{P}_{out}}. \tag{35}$$

When the linear amplification reaches up to the saturation point, the OBO (35) will be equivalent to the IBO (34) and the PAPR (29). Using the relationship of the HPA efficiency and OBO given in [40], (32) and (33) can be rewritten, respectively, as

$$\eta_A = 0.5\frac{1}{PAPR}, \tag{36}$$

and

$$\eta_B = 0.78\frac{1}{PAPR}. \tag{37}$$

From (36) and (37), it can be seen that the PAPR of the signal affects the efficiency of the HPA. Efficiency can be also be improved by reducing the IBO. However, signal that exceeds the saturation point will be clipped and will lead to undesired spectral growth.

C. SPECTRAL REGROWTH

For the sake of simplicity, it is useful to linearize the nonlinearity of the HPA as follows [41]

$$\tilde{S}_n = \alpha S_n + D_n, \tag{38}$$

where S_n and $\tilde{S}_n$ are the Fourier transforms of the HPA input signal $s(t)$ and output signal $\tilde{s}(t)$, respectively. Parameter α represents the attenuation factor and D_n denotes the nonlinear distortion component caused by the HPA. Assuming that D_n and S_n are statistically uncorrelated, the attenuation factor α can be obtained using

$$\alpha = \frac{E\{\tilde{S}_n S_n^\dagger\}}{E\{|S_n|^2\}} = \frac{E\{\tilde{S}_n S_n^\dagger\}}{\mathcal{P}_s}, \tag{39}$$

where $(\cdot)^\dagger$ denotes conjugate, and $\mathcal{P}_s = E\{|S_n|^2\}$ is the average power of S_n.

The average power of the nonlinear distortion component, D_n, can expressed as [41]

$$\tilde{\mathcal{P}}_{d,n} = \tilde{\mathcal{P}}_s - \tilde{\mathcal{P}}_{s,n}, \tag{40}$$

where $\tilde{\mathcal{P}}_{s,n} = \alpha^2\mathcal{P}_s$ is the power of the attenuated signal and $\tilde{\mathcal{P}}_s = E\{|\tilde{S}_n|^2\}$ is the power of the HPA output signal.

Using (40), the spectral regrowth can be measured using the adjacent channel leakage ratio (ACLR) [42] by the ratio of the out-of-band power emission and the in-band signal power, written as [39]

$$ACLR \triangleq \frac{\sum_{n=N}^{3N/2-1}\tilde{\mathcal{P}}_{d,n}}{\sum_{n=\frac{N}{2}}^{N-1}\tilde{\mathcal{P}}_s}. \tag{41}$$

where N is the total number of data symbols.

In this paper, without loss of generality, the ACLR is used to measure the OOB radiation of the signal.

D. EFFECTIVE SNR

The receiver performance can be analyzed by measuring the SNR, which is defined as

$$SNR = \frac{\mathcal{P}_{out}}{\mathcal{P}_z}, \tag{42}$$

where $\mathcal{P}_z$ is the noise power and $\mathcal{P}_{out}$ is the HPA average output power. However, when the HPA power, $\mathcal{P}_{DC}$, in (31) is fixed, a signal with a higher efficiency will achieve a higher average output power, $\mathcal{P}_{out}$. Different systems will have different efficiency at a given IBO or ACLR. Therefore, the receiver performance should be evaluated in a unified manner using the effective SNR, defined as [39]

$$\begin{aligned} SNR_{eff} &= \frac{\mathcal{P}_{DC}}{\mathcal{P}_z} = \frac{\mathcal{P}_{out}}{\eta\mathcal{P}_z} \\ &= \frac{1}{\eta}SNR. \end{aligned} \tag{43}$$

E. SPECTRAL EFFICIENCY

By comparing the transmitted data and recovered data, the spectral efficiency of the system can be evaluated using the average mutual information (AMI) [43]. The AMI, denoted by $I(\mathcal{X};\mathcal{Y})$, measures the dependence of two sets of random variables $\mathcal{X}$ and $\mathcal{Y}$, where $I(\mathcal{X};\mathcal{Y}) = 0$ represents total independence of the random variables. The AMI can be used to measure the spectral efficiency when the signal is transmitted over a wireless channel, such as the AWGN and multipath channels. The spectral efficiency (SE) of the system can be obtained from the AMI as [43],

$$\text{SE} = \text{AMI} = \frac{I(\mathcal{X};\mathcal{Y})}{N}, \tag{44}$$

where

$$I(\mathcal{X};\mathcal{Y}) = \sum_{y\in\mathcal{Y}}\sum_{x\in\mathcal{X}} p(x,y)\log\frac{p(x,y)}{p(x)p(y)}, \tag{45}$$

is the mutual information, $p(x,y)$ is the joint distribution of $\mathcal{X}$ and $\mathcal{Y}$, and $p(x)$ and $p(y)$ are the marginal distributions of $\mathcal{X}$

and $\mathcal{Y}$ respectively. To compute the AMI of the GFDM system using (45), $\mathcal{X}$ is used to represent the input data symbols $\mathbf{x}$ while $\mathcal{Y}$ is the recovered data symbols $\hat{\mathbf{x}}$.

F. ENERGY EFFICIENCY

Complex receivers are often implemented to suppress the self interference due to pulse shaping, as well as nonlinearity distortion by the HPA. Hence, it is essential to analyze the processor power consumption based on the complexity and its spectral efficiency. The energy efficiency (EE) of a system can be measured using [44]

$$\mathrm{EE} = \frac{\Omega(\mathrm{SE})}{\mathcal{P}_c}, \tag{46}$$

where Ω is the total bandwidth occupied, SE is the spectral efficiency of the system, and $\mathcal{P}_c$ is the power consumed from the processing of the signal at both the transmitter and receiver.

VI. NUMERICAL RESULTS

Throughout the simulations, unless specified, the following parameters are used for the GFDM systems: 16-QAM modulation, number of subcarriers $K = 128$, and number of subsymbols $M = 15$. The performance of an OFDM system and GFDM system using RC filter with similar roll-off factor to the designed QP filter is evaluated and compared. In the OFDM system, the subcarriers and subsymbols is set at $K_{ofdm} = K \times M$ and $M_{ofdm} = 1$, respectively. For simplicity, the GFDM with RC filter will be referred to as RC-GFDM, while the GFDM system with the proposed designed pulse shaping filter via the QP optimization approach will be referred to as QP-GFDM.

The desired filter frequency response, $P_d(\omega)$, is chosen to be the frequency response of the RC pulse shaping filter, which is defined as [45]

$$|P_{rc}(f)| = \begin{cases} T, & 0 \le |f| \le \frac{1-\beta}{2T} \\ \frac{T}{2}(1-\sin(\frac{\pi T}{\beta}(|f|-\frac{1}{2T}))), & \frac{1-\beta}{2T} < |f| \le \frac{1+\beta}{2T} \\ 0, & |f| > \frac{1+\beta}{2T}, \end{cases} \tag{47}$$

where T is the symbol interval, and $\beta = 0.2$ is the excess bandwidth of the RC filter. The roll-off factor value has been found through extensive simulations to be optimal in terms of the GFDM system performance. The FIR filter is set at $R = 28$ taps, which is sufficient for designing the FIR filter. A passband tolerance of $\sigma_p = 0.001$ allows the designed filter frequency response to accurately approximate the desired filter without imposing a constraint that is too tight. The discretization parameter L is set to match the filter length for the GFDM system in (3). The filter design parameters are summarized in Table 1. The frequency response of the designed filter illustrated in Fig. 4 has a very close approximate of the RC filter. Fig. 5 illustrates the PSD of the designed pulse shaping filter when used in GFDM, which has a 3 dB lower OOB radiation when compared to the one with ideal RC filter and more than 10 dB lower than the OFDM system. It is worth mentioning that, several other pulse shaping filters exist in the literature and can be selected as the desired filter frequency response, $P_d(\omega)$. The designed filter performance should then be compared with the corresponding desired filter when applied in the GFDM system.

TABLE 1. Filter design parameter settings.

Parameter	Value
Filter taps (R)	28
Passband tolerance (σ_p)	0.001
Discretization param. (L)	$2M$
Discretization param. (q)	8
Desired filter ($P_d(\omega)$)	RC
Filter roll-off factor (β)	0.2

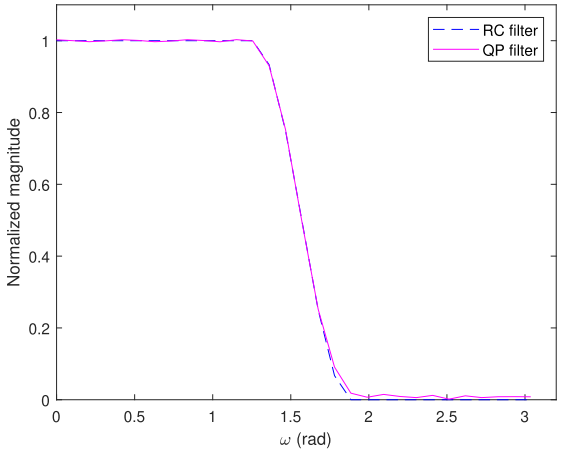

FIGURE 4. Frequency response of designed quadratic programming (QP) pulse shaping filter, compared with the desired filter, raised cosine (RC) filter.

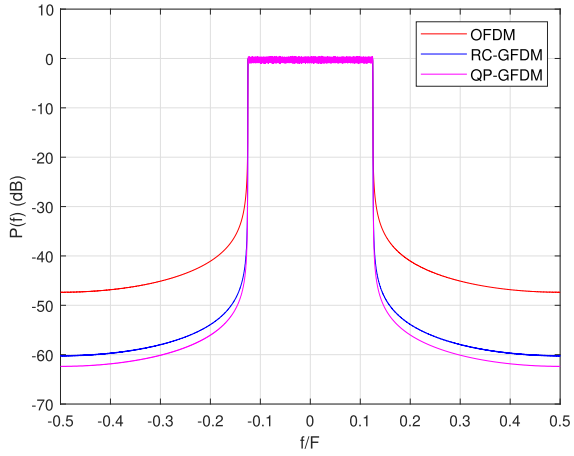

FIGURE 5. OOB radiation of QP-GFDM, compared with RC-GFDM and OFDM.

A. PAPR AND HPA EFFICIENCY

As illustrated in Fig. 6, when considering the PAPR at 10^{-3} probability, the PAPR of QP-GFDM is about 12.2 dB, 0.3 dB

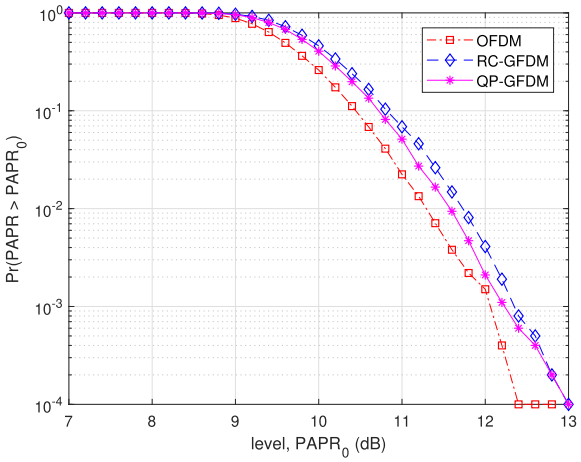

FIGURE 6. CCDF analysis of PAPR of different signals.

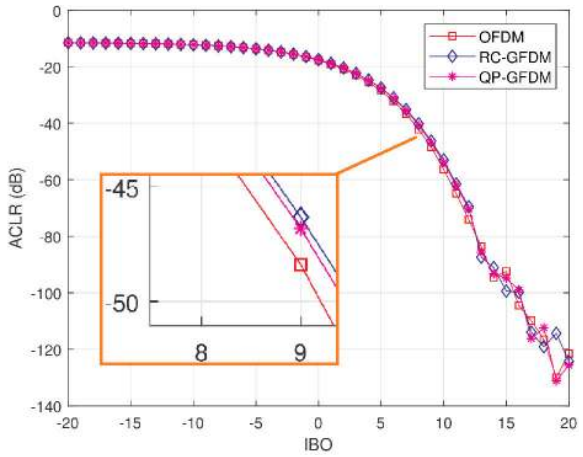

FIGURE 8. Relationship between the IBO level and the ACLR.

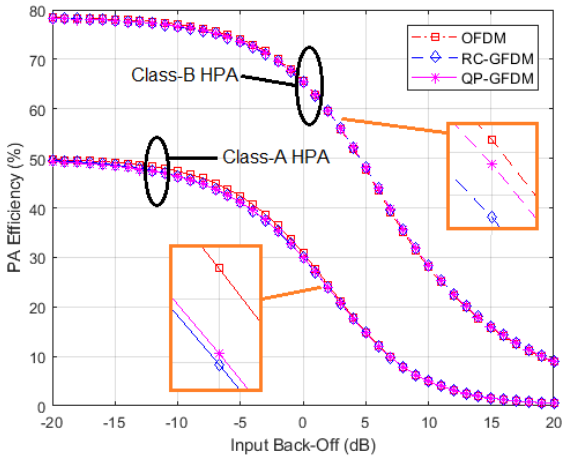

FIGURE 7. Relationship between the IBO level and the efficiency of the designed filter.

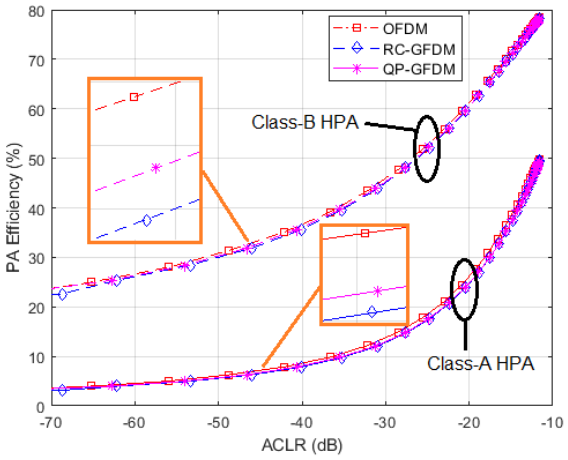

FIGURE 9. Relationship between the ACLR and the HPA efficiency.

lower than RC-GFDM, while OFDM has a PAPR of 12 dB. In general, a lower PAPR will reflect a higher HPA efficiency, as a larger portion of the input power to the HPA, $\mathcal{P}_{DC}$, is used to amplify the input signal. Higher PAPR means lower energy efficiency as power is wasted and dissipated as heat.

As shown in Fig. 7, the OFDM system has a slightly higher HPA efficiency when compared with the GFDM systems. The efficiency difference between RC-GFDM and QP-GFDM is very minimal, with QP-GFDM having a better efficiency performance than RC-GFDM. This is due to the lower PAPR of the QP-GFDM signal when compared to RC-GFDM as shown in Fig. 6.

It can be seen from Fig. 7 that the efficiency of the HPA can go as low as 1% for Class-A amplifier and 9% for Class-B amplifier, when the IBO is increased to allow for the HPA to operate in the linear region. It can also be deduced that the maximum achievable efficiency is achieved when the PAPR approaches unity as a result of lower IBO, with around 50% for Class-A HPA and 78% for Class-B HPA, aligning with (36) and (37) respectively. However, this also means that a greater portion of the signal exceeds the HPA saturation region and is clipped, resulting in spectral regrowth.

B. PSD AND ACLR

Fig. 8 illustrates the ACLR of each signal to show the amount of spectral regrowth due to the HPA nonlinearity, with respect to different levels of IBO. Ideally, the IBO needs to be as low as possible in order to obtain a higher HPA efficiency. On the other hand, the IBO level should be high enough to minimize the ACLR as a result from HPA nonlinearity distortion. To satisfy the 5G-NR specifications, the ACLR is set to be -45 dB [6]. From Fig. 8, any IBO levels of lower than 8.4 dB, 8.7 dB, and 8.6 dB for OFDM, RC-GFDM, and QP-GFDM, respectively, will not be acceptable as the resultant ACLR is greater than -45 dB. In the following numerical simulations, the IBO is set to satisfy the ACLR limit of -45 dB, unless mentioned otherwise.

In Fig. 9, the trade-off between the HPA efficiency and ACLR can be observed, with the IBO as the controlled variable. At ACLR $=$ -45 dB, the efficiency of OFDM, RC-GFDM, and QP-GFDM with Class-A amplifiers are

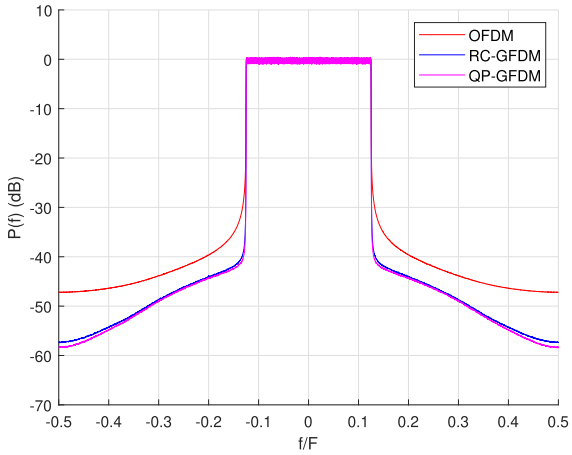

FIGURE 10. Power spectral density of the different signals after HPA nonlinearity.

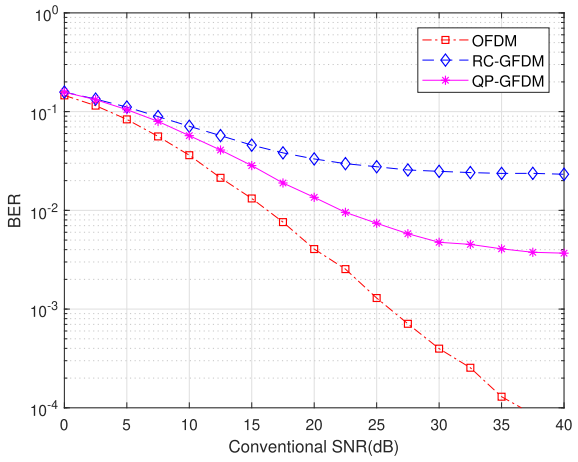

FIGURE 11. BER analysis of GFDM and OFDM signals that are subjected to HPA nonlinearity using conventional SNR.

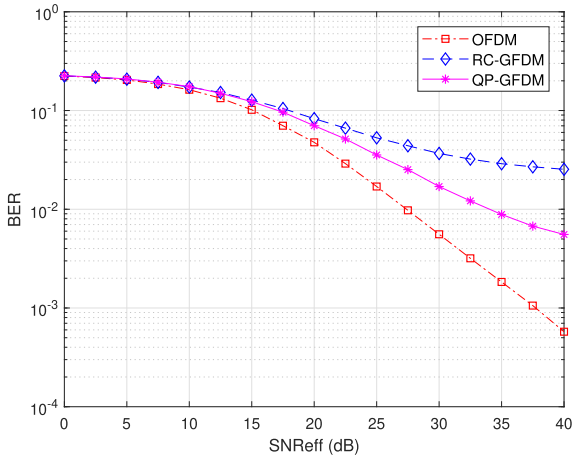

FIGURE 12. BER of GFDM systems with Class-A HPA using the effective SNR measure.

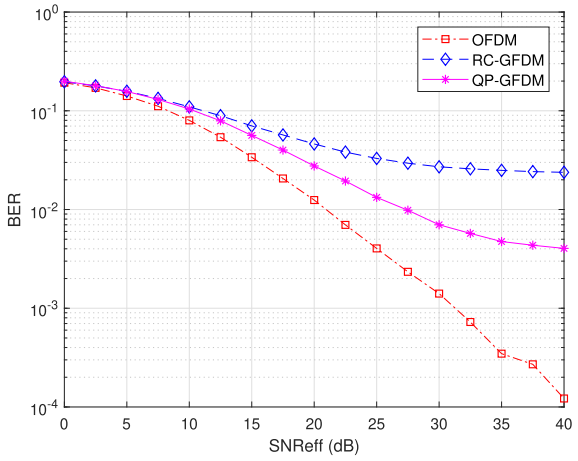

FIGURE 13. BER of GFDM systems using Class-B HPA.

obtained as 7.2%, 6.6%, and 6.7%, respectively, with Class-B amplifiers 33.5%, 32.7%, and 33.0%, respectively. The IBO levels and amplifier efficiencies obtained at ACLR $= -45$ dB can be observed to have a relationship with the PAPR of each respective systems shown in Fig. 6, where a higher PAPR requires a higher IBO, hence a lower HPA efficiency.

To view the effects of HPA nonlinearity from another angle, the PSD before and after HPA is shown in Fig. 10. Although the GFDM signal experienced spectral regrowth, the OOB radiation of the GFDM signal is still lower than OFDM, and is also within acceptable levels. The low OOB radiation is essential in wireless communications, and in particular for IoT networks, as this allows more devices to occupy the channel bandwidth with minimum interference to each other.

C. BER

To analyze the performance of the GFDM system at the receiver, the transmitted signal is passed through a Rayleigh fading channel, where the HIPERLAN/2 Class A [46] channel model is used. The simulations are performed with the assumption that the system has a guard interval larger than the delay spread of the channel, and the receiver has perfect and instantaneous knowledge of the channel state information (CSI).

As shown in Fig. 11, QP-GFDM has a better BER performance as compared with RC-GFDM when analyzed using the conventional signal-to-noise power ratio (SNR). Due to the self interference from pulse shaping in GFDM systems, an error floor exists in the GFDM system, thus the BER of GFDM is often worse than OFDM. Although the MMSE equalizer is applied, it is often not enough to compensate for the distortion due to the HPA nonlinearity.

To present a unified analysis of the BER, the BER performance is evaluated using the effective SNR with Class-A and Class-B amplifiers, shown in Fig. 12 and Fig. 13 respectively. Both analysis show that the BER is increased as compared with using conventional SNR, with systems using Class-A amplifiers having poorer performance.

D. SPECTRAL EFFICIENCY

The spectral efficiency analysis of the OFDM, RC-GFDM, and QP-GFDM for Class-A and Class-B HPA are analyzed

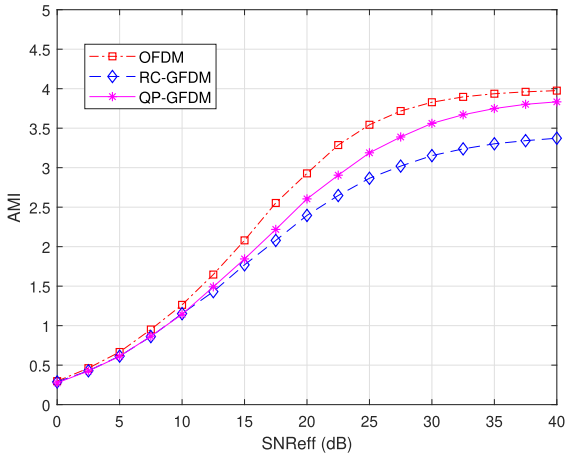

FIGURE 14. AMI of the GFDM systems with Class-A HPA.

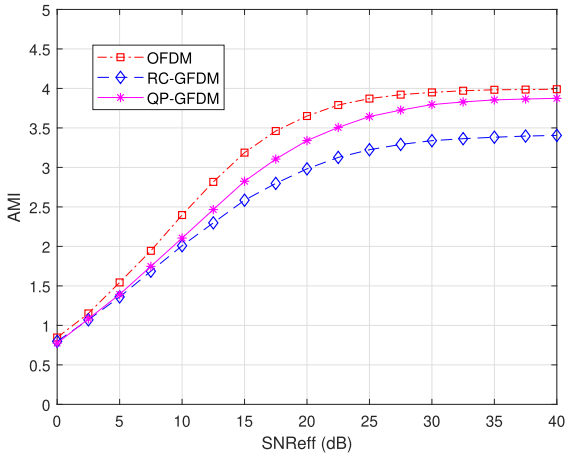

FIGURE 15. AMI of the GFDM systems with Class-B HPA.

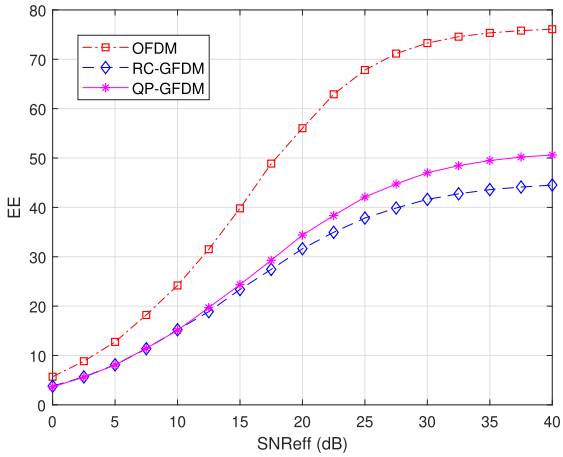

FIGURE 16. Energy efficiency of RC-GFDM and QP-GFDM with Class-A HPA.

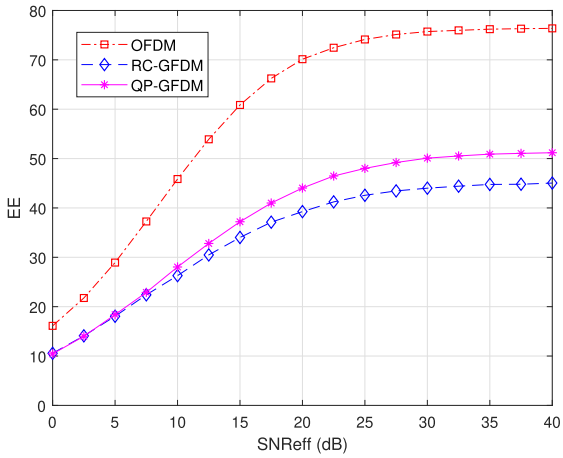

FIGURE 17. Energy efficiency of RC-GFDM and QP-GFDM with Class-B HPA.

using AMI in (45), as shown in Fig. 14 and Fig. 15 respectively. When looking at a particular AMI for systems using Class-A amplifiers, say AMI = 3 bits per sample, the OFDM system is able to achieve such AMI at the lowest SNR_{eff} value of about 20 dB, followed by QP-GFDM and RC-GFDM at about 23 dB and 27 dB respectively. As for systems using Class-B amplifiers, the OFDM system can achieve AMI = 3 at SNR_{eff} = 13 dB, QP-GFDM at 17 dB, and RC-GFDM at 20 dB. This follows from the BER analyzed previously, where a worse BER will have a lower spectral efficiency. It can also be seen from both Fig. 14 and Fig. 15 that the AMI obtained from QP-GFDM approaches the AMI of OFDM at higher SNR_{eff} values.

E. ENERGY EFFICIENCY

The implementation of filtering in GFDM requires additional processing at both the transmitter and receiver, which will increase the power consumption. The power consumption is measured using data from a fixed-point DSP as described in [47]. The energy consumption of the DSP per cycle is $415.8\frac{\text{pWsec}}{\text{cycle}}$, where a complex multiplication requires 3 cycles. The energy consumption per GFDM symbol, $\mathcal{P}_c$, can then be written as

$$\begin{aligned}\mathcal{P}_c &= 415.8\frac{\text{pWsec}}{\text{cycle}}[3(C_{GFDM})]\text{cycle}\\ &= 1.2474[C_{GFDM}]\mu\text{J}.\end{aligned} \tag{48}$$

The complexity of the GFDM system, C_{GFDM}, only considers the fast Fourier transform (FFT) operations and the filter multiplication, where other operations are assumed to be omitted as they can be realized by means of register manipulation. The complexity at the transmitter, $C_{GFDM,Tx}$, and receiver, $C_{GFDM,Rx}$, can be calculated, respectively, using [48], [49]

$$C_{GFDM,Tx} = KM\log_2 M + KVM + N\log_2 N, \tag{49}$$

and

$$C_{GFDM,Rx} = N\log_2 N + KVM + KM\log_2 M, \tag{50}$$

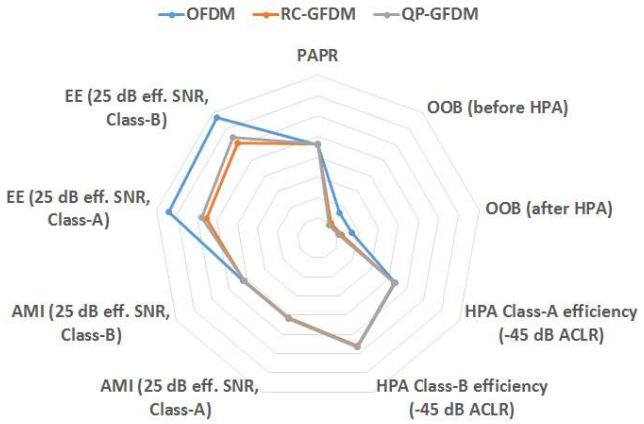

FIGURE 18. Performance comparison of QP-GFDM, RC-GFDM, and OFDM.

where N is the total number of data symbols, K is the number of subcarriers, M is the number of subsymbols, and V is the upsampling factor of the filter.

As illustrated in Fig. 16 and Fig. 17, QP-GFDM has a higher energy efficiency than RC-GFDM by about 7 bits/J for one GFDM sample in both cases with Class-A and Class-B amplifiers.

The performance of the QP-GFDM system compared to the one of RC-GFDM and OFDM is summarized in Fig. 18. In general, the QP-GFDM system has a better performance than the RC-GFDM system when considering the HPA nonlinearity. The OFDM system has a significantly better energy efficiency as compared to QP-GFDM and RC-GFDM, but it has a higher OOB radiation which may interfere with neighbouring channels.

VII. CONCLUSION

In this paper, the pulse shaping filter design using the computationally efficient optimization approach has been presented. The performance of the designed pulse shaping filter in the GFDM system has been analyzed by considering the effects of HPA nonlinearity.

Numerical results have shown that the designed pulse shaping filter has a frequency response that is a close approximate of the ideal RC filter. It has been shown that using the designed filter in GFDM, QP-GFDM, can achieve 3 dB lower OOB radiation level compared to the RC-GFDM, and QP-GFDM has significantly 10 dB lower OOB radiation compared to the OFDM system. Regarding the PAPR, the PAPR of the QP-GFDM is 0.3 dB lower than the RC-GFDM. It has been shown that by varying the IBO, the trade-off between achieving low OOB radiation and high HPA efficiency can be achieved. Following 5G-NR specifications, the ACLR limit has been set at -45 dB and the IBO for each system that satisfies the limit has been obtained. At ACLR $= -45$ dB, it has been shown that QP-GFDM has increased the efficiency of the HPA compared to the RC-GFDM for both Class-A and Class-B amplifiers. Although the HPA nonlinearity may introduce spectral regrowth, the PSD of the GFDM signal shows that the OOB radiation of the distorted GFDM signal is still within acceptable levels, with QP-GFDM having an OOB radiation of about 1 dB lower than RC-GFDM. At the receiver, QP-GFDM is able to achieve significantly lower BER compared to RC-GFDM. However, the BER of QP-GFDM is not lower than OFDM. This may be due to the ISI from using non rectangular pulse shaping filters. QP-GFDM has shown better spectral efficiency where its AMI is around 0.5 bits/sample more than RC-GFDM for both Class-A and Class-B amplifiers. Furthermore, the energy efficiency performance of the QP-GFDM is 7 bits/J per sample higher than the energy efficiency performance of the RC-GFDM at an effective SNR of 40 dB. In summary, the QP-GFDM has shown significant improvement in overall performance compared to RC-GFDM. In future work, designing optimal pulse shaping filters for the 5G-NR waveforms, such as CP-OFDM and DFT-s-OFDM, will be investigated.

REFERENCES

[1] Y. Wu and W. Y. Zou, "Orthogonal frequency division multiplexing: A multi-carrier modulation scheme," *IEEE Trans. Consum. Electron.*, vol. 41, no. 3, pp. 392–399, Aug. 1995.
[2] R. van Nee, G. Awater, M. Morikura, H. Takanashi, M. Webster, and K. W. Halford, "New high-rate wireless LAN standards," *IEEE Commun. Mag.*, vol. 37, no. 12, pp. 82–88, Dec. 1999.
[3] Y. Rahmatallah and S. Mohan, "Peak-to-average power ratio reduction in OFDM systems: A survey and taxonomy," *IEEE Commun. Surveys Tuts.*, vol. 15, no. 4, pp. 1567–1592, Apr. 2013.
[4] A. Osseiran, F. Boccardi, V. Braun, K. Kusume, P. Marsch, M. Maternia, O. Queseth, M. Schellmann, H. Schotten, H. Taoka, H. Tullberg, M. A. Uusitalo, B. Timus, and M. Fallgren, "Scenarios for 5G mobile and wireless communications: The vision of the METIS project," *IEEE Commun. Mag.*, vol. 52, no. 5, pp. 26–35, May 2014.
[5] G. Wunder, P. Jung, M. Kasparick, T. Wild, F. Schaich, Y. Chen, S. Brink, I. Gaspar, N. Michailow, A. Festag, L. Mendes, N. Cassiau, D. Ktenas, M. Dryjanski, S. Pietrzyk, B. Eged, P. Vago, and F. Wiedmann, "5GNOW: non-orthogonal, asynchronous waveforms for future mobile applications," *IEEE Commun. Mag.*, vol. 52, no. 2, pp. 97–105, Feb. 2014.
[6] J. M. Meredith, *NR; Base Station (BS) Radio Transmission and Reception*, document 3GPP TS 38.104 V15.2.0, Jul. 2018.
[7] A. Sahin and H. Arslan, "Edge windowing for OFDM based systems," *IEEE Commun. Lett.*, vol. 15, no. 11, pp. 1208–1211, Nov. 2011.
[8] E. Guvenkaya, E. Bala, R. Yang, and H. Arslan, "Time-asymmetric and subcarrier-specific pulse shaping in OFDM-based waveforms," *IEEE Trans. Veh. Technol.*, vol. 64, no. 11, pp. 5070–5082, Nov. 2015.
[9] R.-A. Pitaval and B. M. Popovic, "Filtered-prefix OFDM," *IEEE Commun. Lett.*, vol. 23, no. 1, pp. 28–31, Jan. 2019.
[10] T. Matsuura, Y. Iida, C. Han, and T. Hashimoto, "Improved algorithms for cancellation carrier optimization to suppress the OFDM OOB spectrum," *IEEE Commun. Lett.*, vol. 13, no. 2, pp. 112–114, Feb. 2009.
[11] A. Selim and L. Doyle, "Out-of-band interference reduction using subcarrier weighting and cancellation carriers," in *Proc. IEEE 79th Veh. Technol. Conf. (VTC Spring)*, May 2014, pp. 1–5.
[12] B. Farhang-Boroujeny, "OFDM versus filter bank multicarrier," *IEEE Signal Process. Mag.*, vol. 28, no. 3, pp. 92–112, May 2011.
[13] V. Vakilian, T. Wild, F. Schaich, S. ten Brink, and J.-F. Frigon, "Universal-filtered multi-carrier technique for wireless systems beyond LTE," in *Proc. IEEE Globecom Workshops (GC Wkshps)*, Dec. 2013, pp. 223–228.
[14] G. Fettweis, M. Krondorf, and S. Bittner, "GFDM—Generalized frequency division multiplexing," in *Proc. IEEE 69th Veh. Technol. Conf. (VTC Spring)*, Apr. 2009, pp. 1–4.
[15] M. Matthe, N. Michailow, I. Gaspar, and G. Fettweis, "Influence of pulse shaping on bit error rate performance and out of band radiation of generalized frequency division multiplexing," in *Proc. IEEE Int. Conf. Commun. Workshops (ICC)*, Jun. 2014, pp. 43–48.

[16] A. Kumar and M. Magarini, "Improved nyquist pulse shaping filters for generalized frequency division multiplexing," in *Proc. 8th IEEE Latin-Amer. Conf. Commun. (LATINCOM)*, Nov. 2016, pp. 1–7.
[17] P. Kumar, L. Kansal, G. S. Gaba, M. El Bakkali, F. Tubbal, and S. Abulgasem, "BER analysis of GFDM system augmented with SC diversity combining scheme for diverse pulse shaping filters," in *Proc. 12th Int. Conf. Telecommun. Syst., Services, Appl. (TSSA)*, Oct. 2018, pp. 1–6.
[18] C.-Y. Lin, Y. Huang, and B. Su, "Prototype filter design in GFDM systems in presence of PA nonlinearity," in *Proc. IEEE 23rd Int. Conf. Digit. Signal Process. (DSP)*, Nov. 2018, pp. 1–5.
[19] P.-C. Chen and B. Su, "Filter optimization of out-of-band radiation with performance constraints for GFDM systems," in *Proc. IEEE 18th Int. Workshop Signal Process. Adv. Wireless Commun. (SPAWC)*, Jul. 2017, pp. 1–5.
[20] R. Reine and Z. Zang, "A quadratic programming approach in pulse shaping filter design to reducing PAPR in OFDM systems," in *Proc. 19th Asia–Pacific Conf. Commun.(APCC)*, Aug. 2013, pp. 572–576.
[21] Z. A. Sim, R. Reine, Z. Zang, F. H. Juwono, and L. Gopal, "Reducing the PAPR of GFDM systems with quadratic programming filter design," in *Proc. IEEE 89th Veh. Technol. Conf. (VTC-Spring)*, Apr. 2019, pp. 1–5.
[22] Z. A. Sim, F. H. Juwono, R. Reine, Z. Zang, and L. Gopal, "Reducing out-of-band radiation in GFDM systems using pulse shaping filter design," presented at the 25th Asia–Pacific Conf. Commun. (APCC), Nov. 2019.
[23] A. Ortega, L. Fabbri, and V. Tralli, "Performance evaluation of GFDM over nonlinear channel," in *Proc. Int. Conf. Inf. Commun. Technol. Converg. (ICTC)*, Oct. 2016, pp. 12–17.
[24] A. Mohammadian, A. Mohammadi, A. Abdipour, and M. Baghani, "Spectral analysis of GFDM modulated signal under nonlinear behavior of power amplifier," 2018, *arXiv:1803.02026*. [Online]. Available: http://arxiv.org/abs/1803.02026
[25] L. Sendrei and S. Marchevský, "On the performance of GFDM systems undergoing nonlinear amplification," *Acta Electrotechnica et Inf.*, vol. 15, no. 1, pp. 9–14, Mar. 2015.
[26] N. Michailow and G. Fettweis, "Low peak-to-average power ratio for next generation cellular systems with generalized frequency division multiplexing," in *Proc. Int. Symp. Intell. Signal Process. Commun. Syst.*, Nov. 2013, pp. 651–655.
[27] H. Ochiai, "An analysis of band-limited communication systems from amplifier efficiency and distortion perspective," *IEEE Trans. Commun.*, vol. 61, no. 4, pp. 1460–1472, Apr. 2013.
[28] C. Rapp, "Effects of HPA-nonlinearity on 4-DPSK/OFDM-signal for a digital sound broadcasting system," in *Proc. 2nd ECSC*, Oct. 1991, pp. 179–184.
[29] S. Teodoro, A. Silva, R. Dinis, F. M. Barradas, P. M. Cabral, and A. Gameiro, "Theoretical analysis of nonlinear amplification effects in massive MIMO systems," *IEEE Access*, vol. 7, pp. 172277–172289, 2019.
[30] J. Joung, C. K. Ho, K. Adachi, and S. Sun, "A survey on power-amplifier-centric techniques for spectrum- and energy-efficient wireless communications," *IEEE Commun. Surveys Tuts.*, vol. 17, no. 1, pp. 315–333, 1st Quart., 2015.
[31] R. Zayani, H. Shaiek, and D. Roviras, "Efficient precoding for massive MIMO downlink under PA nonlinearities," *IEEE Commun. Lett.*, vol. 23, no. 9, pp. 1611–1615, Sep. 2019.
[32] G. U. Maheswari, A. Govindasamy, and S. J. Thiruvengadam, "Performance analysis of filter bank multicarrier system with non-linear high power amplifiers for 5G wireless networks," *IET Signal Process.*, vol. 11, no. 1, pp. 66–72, Feb. 2017.
[33] *Realistic Power Amplifier Model for the New Radio Evaluation*, document R4-163314, 3GPP, TSG-RAN WG4 Meeting 79, Nokia, May 2016.
[34] T. van Waterschoot, V. Le Nir, J. Duplicy, and M. Moonen, "Analytical expressions for the power spectral density of CP-OFDM and ZP-OFDM signals," *IEEE Signal Process. Lett.*, vol. 17, no. 4, pp. 371–374, Apr. 2010.
[35] Z. Zang and S. Nordholm, "Design of ODMA digital waveforms using non-convex optimization methods," *Ann. Oper. Res.*, vol. 133, nos. 1–4, pp. 319–330, Jan. 2005.
[36] R. L. Streit and A. H. Nuttall, "A note on the semi-infinite programming approach to complex approximation," *Math. Comput.*, vol. 40, no. 162, pp. 599–605, Jan. 1983.
[37] N. Michailow, M. Matthe, I. S. Gaspar, A. N. Caldevilla, L. L. Mendes, A. Festag, and G. Fettweis, "Generalized frequency division multiplexing for 5th generation cellular networks," *IEEE Trans. Commun.*, vol. 62, no. 9, pp. 3045–3061, Sep. 2014.
[38] Y. S. Cho, J. Kim, W. Y. Yang, and C. G. Kang, *MIMO-OFDM Wireless Communications With MATLAB*, 1st ed. Hoboken, NJ, USA: Wiley, 2010.
[39] R. Yoshizawa and H. Ochiai, "Energy efficiency improvement of coded OFDM systems based on PAPR reduction," *IEEE Syst. J.*, vol. 11, no. 2, pp. 717–728, Jun. 2017.
[40] A. Cheaito, J.-F. Hélard, M. Crussière, and Y. Louët, "EVM derivation of multicarrier signals to determine the operating point of the power amplifier considering clipping and predistortion," *EURASIP J. Wireless Commun. Netw.*, vol. 2016, no. 1, p. 281, Dec. 2016.
[41] H. Ochiai and H. Imai, "Performance analysis of deliberately clipped OFDM signals," *IEEE Trans. Commun.*, vol. 50, no. 1, pp. 89–101, Jan. 2002.
[42] T. J. Rouphael, *RF and Digital Signal Processing for Software-Defined Radio*. Burlington, VT, USA: Newnes, 2009.
[43] J. Joung, C. Keong Ho, and S. Sun, "Spectral efficiency and energy efficiency of OFDM systems: Impact of power amplifiers and countermeasures," *IEEE J. Sel. Areas Commun.*, vol. 32, no. 2, pp. 208–220, Feb. 2014.
[44] Y. Chen, S. Zhang, S. Xu, and G. Li, "Fundamental trade-offs on green wireless networks," *IEEE Commun. Mag.*, vol. 49, no. 6, pp. 30–37, Jun. 2011.
[45] S. Daumont, B. Rihawi, and Y. Lout, "Root-raised cosine filter influences on PAPR distribution of single carrier signals," in *Proc. 3rd Int. Symp. Commun., Control Signal Process.*, Mar. 2008, pp. 841–845.
[46] J. Medbo, H. Andersson, P. Schramm, H. Asplund, and J. E. Berg, *Channel models for HIPERLAN/2 in different indoor scenarios*, document ETSI BRAN 3ERI085B, Mar. 1998.
[47] R. J. Baxley and G. T. Zhou, "Power savings analysis of peak-to-average power ratio reduction in OFDM," *IEEE Trans. Consum. Electron.*, vol. 50, no. 3, pp. 792–798, Aug. 2004.
[48] N. Michailow, I. Gaspar, S. Krone, M. Lentmaier, and G. Fettweis, "Generalized frequency division multiplexing: Analysis of an alternative multi-carrier technique for next generation cellular systems," in *Proc. Int. Symp. Wireless Commun. Syst. (ISWCS)*, Aug. 2012, pp. 171–175.
[49] I. Gaspar, N. Michailow, A. Navarro, E. Ohlmer, S. Krone, and G. Fettweis, "Low complexity GFDM receiver based on sparse frequency domain processing," in *Proc. IEEE 77th Veh. Technol. Conf. (VTC Spring)*, Jun. 2013, pp. 1–6.

ZEE ANG SIM (Member, IEEE) received the B.Eng. degree in electronic and communications engineering from Curtin University Malaysia, Miri, Malaysia, in 2015, where he is currently pursuing the Ph.D. degree in electrical and computer engineering. His research interests include signal processing for communications, wireless communications, and filter design for communication systems.

FILBERT H. JUWONO (Senior Member, IEEE) received the B.Eng. degree in electrical engineering and the M.Eng. degree in telecommunication engineering from the University of Indonesia, Depok, Indonesia, in 2007 and 2009, respectively, and the Ph.D. degree in electrical and electronic engineering from The University of Western Australia, Perth, WA, Australia, in 2017. He is currently a Lecturer with the Department of Electrical and Computer Engineering, Curtin University Malaysia. His research interests include signal processing for communications, wireless communications, power-line communications, and biomedical engineering. He was a recipient of the prestigious Australian Awards Scholarship, in 2012. He serves as an Associate Editor for IEEE Access.

REGINA REINE (Member, IEEE) received the B.Eng. degree in electrical engineering from Trisakti University, Jakarta, Indonesia, in 2000, the M.Sc. degree in computation engineering from UMIST, Manchester, U.K., in 2002, the M.Sc. degree in electrical engineering from the University of Aberdeen, Scotland, U.K., in 2004, and the Ph.D. degree in electrical engineering from Curtin University Malaysia, in 2016. She is currently a Lecturer with the Department of Electrical Engineering, Curtin University Malaysia. Her research interests include wireless communications, power-line communications, and unmanned aerial vehicles.

ZHUQUAN ZANG (Member, IEEE) received the B.Sc. degree from Shandong Normal University, Jinan, China, the M.Sc. degree from Shandong University, Jinan, and the Ph.D. degree in systems engineering from The Australian National University, Canberra, ACT, Australia, in 1993. From 1993 to 1994, he worked as a Research Associate in optimization, optimal control, and system identification with The University of Western Australia, Perth, WA, Australia. From 1994 to 2002, he worked first as a Research Fellow and then as a Senior Research Fellow with the Australian Telecommunications Research Institute, Curtin University, Perth, WA, Australia. From 2002 to 2005, he worked with the Western Australian Telecommunications Research Institute (a joint venture between Curtin University and The University of Western Australia). During this period, he was with the Australian Telecommunications Cooperative Research Centre. Since 2006, he has been with the Faculty of Engineering and Science, Curtin University Malaysia. His main research interests are in the areas of constrained filter set design for bandwidth-efficient wireless multiuser communications, wideband waveform design for radar and sonar, computationally efficient optimization methods and their application to effective multiscale control scheme design, peak-to-average power ratio (PAPR) reduction in multiple-input–multiple-output (MIMO) orthogonal frequency-division multiplexing (OFDM) systems, and robust transceiver design for non-regenerative MIMO wireless communication systems.

LENIN GOPAL (Member, IEEE) received the B.Eng. degree in electrical and electronics engineering from Madurai Kamaraj University, Madurai, India, in 1996, the M.Eng. degree in telecommunications engineering from Multimedia University, Cyberjaya, Malaysia, in 2006, and the Ph.D. degree from Curtin University, Bentley, WA, Australia, in 2015. He is currently an Associate Professor with the Department of Electrical and Computer Engineering, Faculty of Engineering and Science, Curtin University Malaysia, Miri, Malaysia. His research interests include signal processing for communications, wireless communications, power-line communications, and the Internet of Things (IoT).